Progress In Electromagnetics Research, PIER 92, 1–16, 2009

ANALYTICAL CALCULATION OF MAGNETIC FIELD DISTRIBUTION IN COAXIAL MAGNETIC GEARS

L. Jian and K. T. Chau

Department of Electrical and Electronic Engineering
The University of Hong Kong
Pokfulam Road, Hong Kong, China

Abstract—Coaxial magnetic gears are a new breed of magnetic devices, which utilize the interaction of permanent magnet fields to enable torque transmission. Apart from using a numerical approach for their magnetic field analysis, an analytical approach is highly desirable since it can provide an insightful knowledge for design and optimization. In this paper, a new analytical approach is proposed to calculate the magnetic field distribution in coaxial magnetic gears. A set of partial differential equations in terms of scalar magnetic potential is used to describe the field behavior, and the solution is determined by considering the boundary constraints. The accuracy of the proposed approach is verified by comparing the field distribution results with those obtained from the finite element method.

1. INTRODUCTION

Coaxial magnetic gear is an emerging magnetic device which can achieve torque transmission and speed variation by the interaction of permanent magnets (PMs) [1–3]. Due to its non-contact mechanism, it can offer some distinct advantages over the mechanical gearboxes, namely the minimum acoustic noise, free from maintenance, improved reliability, inherent overload protection, and physical isolation between input and output shafts. Moreover, since it adopts coaxial topology, the utilization of the PMs can be greatly improved, thus it can offer much higher torque density than the parallel-axis magnetic gears [4]. Also, the coaxial topology makes it readily be integrated with electric machinery to meet the demands arising from wind power generation [5] or electric vehicles [6].

Corresponding author: L. Jian (lnjian@eee.hku.hk).

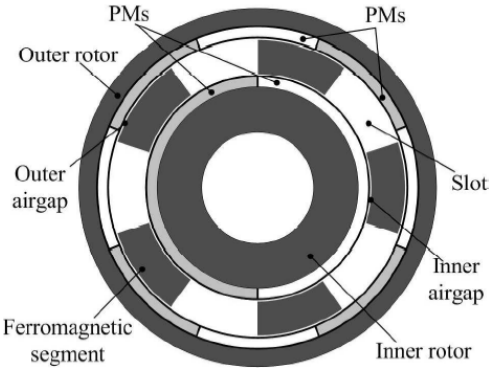

Figure 1. Coaxial magnetic gear.

Figure 1 shows the topology of a typical coaxial magnetic gear. It consists of three main parts: the inner rotor, the stationary ring and the outer rotor. Two airgaps are formed to separate them from each other. PMs are mounted on the surfaces of the two rotors. The stationary ring consists of ferromagnetic segments to modulate the magnetic field built up by the two rotors. For this magnetic gear, the pole-pair numbers of the inner and outer rotors are 1 and 4, respectively. The number of the ferromagnetic segments is 5. Thus, the gear ratio of 4 : 1 is resulted.

An insightful knowledge of the magnetic field distributions in coaxial magnetic gears is vitally important for their design and optimization. As a popular technique for analyzing electromagnetic devices [7, 8], the finite element method (FEM) is also employed to analyze coaxial magnetic gears. However, such numerical method can provide neither closed-form solution nor physical insight for designers. In recent years, the development of analytical approaches to calculate the magnetic field in PM materials [9–12] and PM machines [13] has taken on an accelerated pace.

The purpose of this paper is to propose a new analytical approach to calculate the magnetic field distribution of coaxial magnetic gears. In order to give accurate prediction for both the radial magnetic flux density and the tangential magnetic flux density in the two airgaps, the modulation effect arising from the stationary ring will be modeled by a set of partial differential equations in terms of scalar magnetic potential. The accuracy of the proposed analytical calculation will be verified by comparing the corresponding numerical results with the FEM results.

2. ANALYTICAL MODEL

In order to formulate the analytical model, the permeabilities of the iron yokes of the two rotors and the ferromagnetic segments are assumed to be infinite. Hence, the nonlinear factors are absent, and the magnetic field excited by the two rotors can be considered as superposition of the fields excited by individual rotors. With the outer rotor PMs removed, the magnetic gear illustrated in Fig. 1 can be represented in pseudo-polar coordinates as shown in Fig. 2. The calculation region can be classified into four regions: PMs (Region I), inner airgap (Region II), outer space (Region III), and slots (Region j, $j = 1 - 5$).

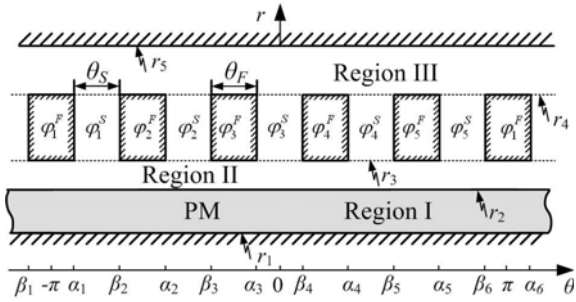

Figure 2. Analytical model.

In various regions, the flux density and field intensity are expressed as:

In Region I:

$$\overline{B} = \mu_0 \mu_r \overline{H} + \mu_0 \overline{M} \tag{1}$$

In Regions II, III and j:

$$\overline{B} = \mu_0 \overline{H} \tag{2}$$

where μ_r is the relative permeability and $\overline{M}$ is the residual magnetization vector of PMs. By using the scalar magnetic potential φ, the field behavior can be governed by a set of 2-rank partial differential equations:

In Region I:

$$\nabla^2 \varphi^I(r, \theta) = \frac{\mathrm{div}\overline{M}}{\mu_r} \tag{3}$$

In Region II:

$$\nabla^2 \varphi^{II}(r, \theta) = 0 \tag{4}$$

In Region III:

$$\nabla^2 \varphi^{III}(r,\theta) = 0 \tag{5}$$

In Region j:

$$\nabla^2 \varphi_j^S(r,\theta) = 0 \tag{6}$$

In order to solve the above equations, the following boundary conditions need to be taken into account:

When $r = r_1$:

$$\varphi^I(r_1,\theta) = 0 \tag{7}$$

When $r = r_2$:

$$\varphi^I(r_2,\theta) = \varphi^{II}(r_2,\theta) \tag{8}$$

$$\mu_r \frac{\partial \varphi^{II}}{\partial r}\Big|_{r=r_2} = \mu_r \frac{\partial \varphi^I}{\partial r}\Big|_{r=r_2} - M_r \tag{9}$$

When $r = r_3$ and $\theta \in [\alpha_j, \beta_{j+1}]$:

$$\varphi^{II}(r_3,\theta) = \varphi_j^S(r_3,\theta) \tag{10}$$

$$\frac{\partial \varphi^{II}}{\partial r}\Big|_{r=r_3} = \frac{\partial \varphi_j^S}{\partial r}\Big|_{r=r_3} \tag{11}$$

When $r = r_3$ and $\theta \in [\beta_j, \alpha_j]$:

$$\varphi^{II}(r_3,\theta) = \varphi_j^F \tag{12}$$

When $\theta = \alpha_j$ and $r \in [r_3, r_4]$:

$$\varphi_j^S(r,\alpha_j) = \varphi_j^F \tag{13}$$

When $\theta = \beta_j$ and $r \in [r_3, r_4]$:

$$\varphi_j^S(r,\beta_j) = \varphi_j^F \tag{14}$$

When $r = r_4$ and $\theta \in [\alpha_j, \beta_{j+1}]$:

$$\varphi^{III}(r_4,\theta) = \varphi_j^S(r_4,\theta) \tag{15}$$

$$\frac{\partial \varphi^{III}}{\partial r}\Big|_{r=r_4} = \frac{\partial \varphi_j^S}{\partial r}\Big|_{r=r_4} \tag{16}$$

When $r = r_4$ and $\theta \in [\beta_j, \alpha_j]$:

$$\varphi^{III}(r_4,\theta) = \varphi_j^F \tag{17}$$

When $r = r_5$:

$$\varphi^{III}(r_5, \theta) = 0 \tag{18}$$

where r_1, r_2, r_3, r_4 and r_5 are the radii of the inner rotor yoke, inner rotor PM surface, stationary ring inside surface, stationary ring outside surface, and outer rotor yoke, respectively; α_j, β_{j+1} are the left border and right border of the jth slot; θ_S, θ_F are the width of the slot and the ferromagnetic segment. Because of the infinite permeability, each ferromagnetic segment can be considered as an equipotential object, and the scalar magnetic potential of the jth segment is denoted by φ_j^F. It should be noted that the 6th and the 1st segments are actually identical, thus having the same potential.

3. MAGNETIC FIELD SOLUTION

3.1. Field Distribution in Airspaces

The scalar magnetic potentials in Region II and III are governed by Laplace's equations given in (4) and (5). By separating the variables r and θ, the general solution in polar coordinates can be written as:

$$\varphi^{II} = \sum_{n=1}^{\infty} \left[\left(E_n r^n + F_n r^{-n} \right) \cos n\theta + \left(G_n r^n + H_n r^{-n} \right) \sin n\theta \right] + E_0 \ln r + F_0 \tag{19}$$

$$\varphi^{III} = \sum_{n=1}^{\infty} \left[\left(I_n r^n + J_n r^{-n} \right) \cos n\theta + \left(K_n r^n + L_n r^{-n} \right) \sin n\theta \right] + I_0 \ln r + J_0 \tag{20}$$

It should be noted that the zero harmonic terms have to be taken into account because of the non-uniformity along the circumference arising from the ferromagnetic segments. Moreover, considering the periodicity, the zero harmonic terms should not be related to θ.

3.2. Field Distribution in PMs

The scalar magnetic potentials in Region I is governed by Poissonian equation given in (3). According to the superposition law, the general solution of Poissonian equation is the sum of the general solution of the corresponding Laplace's equation and one special solution of its own. Fig. 3 shows the magnetization distribution of the PM on the inner rotor, where p is the number of pole-paris and θ_0 is the initail phase angle. In polar coordinates, the magnetization is given by:

$$\overline{M} = M_r \overline{r} + M_\theta \overline{\theta} \tag{21}$$

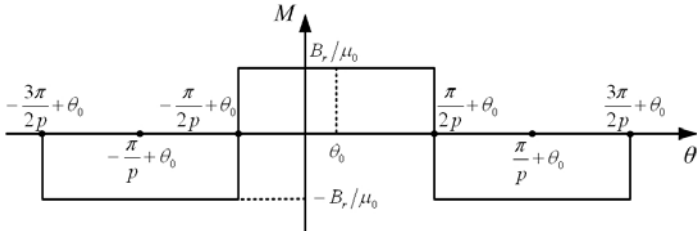

Figure 3. Magnetization distribution.

where $M_\theta = 0$, $M_r = \sum_{n=1}^{\infty} (M_n \cos n\theta_0 \cos n\theta + M_n \sin n\theta_0 \sin n\theta)$ and $M_n = \begin{cases} 4B_r \sin(i\pi/2)/(\mu_0 i\pi) & \text{if } n = ip,\ i = 1, 3, 5, \ldots \\ 0 & \text{otherwise} \end{cases}$. Then, it is easy to find a special solution of (3) as given by:

$$\phi^I = \sum_{n=1}^{\infty} [W_n(r) \cos n\theta_0 \cos n\theta + W_n(r) \sin n\theta_0 \sin n\theta] \tag{22}$$

where

$$W_n(r) = \begin{cases} M_n r / \left(\mu_r \left(1 - n^2\right)\right) & \text{if } n = ip \bigcap p \neq 1,\ i = 1, 3, 5, \ldots \\ M_1 r \ln r/(2\mu_r) & \text{else if } n = p = 1 \\ 0 & \text{otherwise} \end{cases}.$$

Thus, the general solution of the scalar magnetic potential in Region I can be expressed as:

$$\varphi^I = \sum_{n=1}^{\infty} \left[\begin{array}{l} (A_n r^n + B_n r^{-n} + W_n(r) \cos n\theta_0) \cos n\theta \\ +(C_n r^n + D_n r^{-n} + W_n(r) \sin n\theta_0) \sin n\theta \end{array} \right] + A_0 \ln r + B_0 \tag{23}$$

For the same reason as aforementioned, the zero harmonic terms have been taken into account.

3.3. Field Distribution in Slots

The scalar magnetic potential in Region j (the jth slot) is governed by Laplace's equation in (6). Considering the boundary conditions given by (13) and (14), the general solution can not be directly obtained by using the method of separating variables. In order to figure out its general solution, the problem described by (6) and (10)–(17) is separated into the following two cases:

Case 1: Find the solution of the following equation:

$$\nabla^2 \varphi_{j1}^S(r, \theta) = 0 \tag{24}$$

subject to following boundary conditions:

$$\varphi_{j1}^{S}\Big|_{\theta=\beta_j} = \varphi_j^F \tag{25}$$

$$\varphi_{j1}^{S}\Big|_{\theta=\alpha_j} = \varphi_{j+1}^F \tag{26}$$

$$\varphi_{j1}^{S}\Big|_{r=r_3} = \varphi_{j1}^{S}\Big|_{r=r_4} = \varphi_j \tag{27}$$

$$\frac{\partial\varphi_{j1}^{S}}{\delta r}\Big|_{r=r_3} = \frac{\partial\varphi_{j1}^{S}}{\delta r}\Big|_{r=r_4} = 0 \tag{28}$$

where $\varphi_j = a_j\theta + b_j$, $a_j = (\varphi_{j+1}^F - \varphi_j^F)/\theta_S$ and $b_j = (\varphi_j^F\beta_{j+1} - \varphi_j^F\alpha_j)/\theta_S$.

Case 2: Find the solution of the following equation:

$$\nabla^2\varphi_{j2}^{S}(r,\theta) = 0 \tag{29}$$

subject to following boundary conditions:

$$\varphi_{j1}^{S}\Big|_{\theta=\beta_j} = \varphi_{j1}^{S}\Big|_{\theta=\alpha_j} = 0 \tag{30}$$

$$\varphi_{j2}^{S}\Big|_{r=r_3} = \varphi^{II}\Big|_{r=r_3} - \varphi_j \tag{31}$$

$$\varphi_{j2}^{S}\Big|_{r=r_4} = \varphi^{III}\Big|_{r=r_4} - \varphi_j \tag{32}$$

$$\frac{\partial\varphi_{j2}^{S}}{\partial r}\Big|_{r=r_3} = \frac{\partial\varphi^{II}}{\partial r}\Big|_{r=r_3} \tag{33}$$

$$\frac{\partial\varphi_{j2}^{S}}{\partial r}\Big|_{r=r_4} = \frac{\partial\varphi^{III}}{\partial r}\Big|_{r=r_4} \tag{34}$$

These two cases are illustrated in Fig. 4. For Case 1, it is easy to find the general solution as given by:

$$\varphi_{j1}^{S} = a_j\theta + b_j \tag{35}$$

For Case 2, the method of separating variables is suitable for finding its general solution. The corresponding result is given by:

$$\varphi_{j2}^{S} = \sum_{m=1}^{\infty}\left[\left(X_{jm}r^{\lambda_m} + Y_{jm}r^{-\lambda_m}\right)\sin n\lambda_m\left(\theta - \alpha_j\right)\right] \tag{36}$$

where $\lambda_m = m\pi/\theta_S$.

Therefore, the general solution of the scalar magnetic potential in Region j can be expressed as:

$$\varphi_j^S = \varphi_{j1}^S + \varphi_{j2}^S = a_j\theta + b_j + \sum_{m=1}^{\infty}\left[\left(X_{jm}r^{\lambda_m} + Y_{jm}r^{-\lambda_m}\right)\sin n\lambda_m(\theta - \alpha_j)\right] \tag{37}$$

3.4. Boundary Conditions

Firstly, on the surface of the inner rotor yoke, from (7) and (23), it yields:

$$A_n r_1^n + B_n r_1^{-n} + W_n(r_1)\cos n\theta_0 = 0 \tag{38}$$

$$C_n r_1^n + D_n r_1^{-n} + W_n(r_1)\sin n\theta_0 = 0 \tag{39}$$

$$A_0 \ln r_1 + B_0 = 0 \tag{40}$$

Secondly, on the surface of the inner rotor PM, from (8), (9), (19) and (23), it yields:

$$A_n r_2^n + B_n r_2^{-n} + W_n(r_2)\cos n\theta_0 = E_n r_2^n + F_n r_2^{-n} \tag{41}$$

$$C_n r_2^n + D_n r_2^{-n} + W_n(r_2)\sin n\theta_0 = G_n r_2^n + H_n r_2^{-n} \tag{42}$$

$$A_0 \ln r_2 + B_0 = E_0 \ln r_2 + F_0 \tag{43}$$

$$nE_n r_2^n - nF_n r_2^{-n} = \begin{bmatrix} nA_n r_2^n - nB_n r_2^{-n} + r_2 W_n'(r_2)\cos n\theta_0 \\ -r_2 M_n \cos n\theta_0/\mu_r \end{bmatrix} \tag{44}$$

$$nG_n r_2^n - nH_n r_2^{-n} = \begin{bmatrix} nC_n r_2^n - nD_n r_2^{-n} + r_2 W_n'(r_2)\sin n\theta_0 \\ -r_2 M_n \sin n\theta_0/\mu_r \end{bmatrix} \tag{45}$$

$$A_0 = E_0 \tag{46}$$

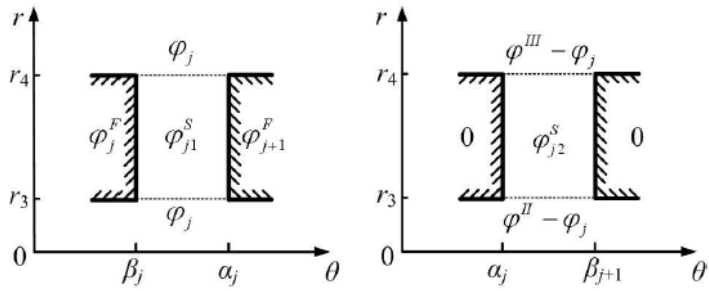

Figure 4. Decomposition of magnetic field in slot: (a) Case 1, (b) Case 2.

Thirdly, on the surface of the outer rotor yoke, from (18) and (20), it yields:

$$I_n r_5^n + J_n r_5^{-n} = 0 \tag{47}$$

$$K_n r_5^n + L_n r_5^{-n} = 0 \tag{48}$$

$$I_0 \ln r_5 + J_0 = 0 \tag{49}$$

Fourthly, on the inside surface of the stationary ring, from (10) and (12), the scalar magnetic potential on this surface can also be expressed as:

$$\varphi^{II}(r_3,\theta) = \begin{cases} \varphi_1^F & \text{if } -\pi \le \theta < \alpha_1 \\ \varphi_j^S(r_3) & \text{if } \alpha_j \le \theta < \beta_{j+1} \\ \varphi_j^F & \text{if } \beta_j \le \theta < \alpha_j \\ \varphi_1^F & \text{if } \beta_6 \le \theta < \pi \end{cases} \tag{50}$$

Expanding (50) into Fourier series over $[-\pi, \pi]$, it yields:

$$\varphi^{II}(r_3,\theta) = \frac{c_0}{2} + \sum_{n=1}^{\infty}[c_n \cos n\theta + d_n \sin n\theta] \tag{51}$$

where

$$c_0 = \left[\begin{array}{l} \sum\limits_{j=1}^{N_S} \sum\limits_{m=1}^{\infty} (1-\cos m\pi)\left(X_{jm} r_3^{\lambda_m} + Y_{jm} r_3^{-\lambda_m}\right)/\lambda_m \\ +T \sum\limits_{j=1}^{N_S} \varphi_j^F \end{array} \right] /\pi,$$

$$c_n = \left[\begin{array}{l} \sum\limits_{j=1}^{N_S} \sum\limits_{m=1}^{\infty} \tau_{nmj}\left(X_{jm} r_3^{\lambda_m} + Y_{jm} r_3^{-\lambda_m}\right) \\ -\sum\limits_{j=1}^{N_S} 2\sin(n\gamma_j)\sin(n\theta_S/2)(\varphi_{j+1}^F - \varphi_j^F)/(n^2\theta_S) \end{array} \right] /\pi,$$

$$d_n = \left[\begin{array}{l} \sum\limits_{j=1}^{N_S} \sum\limits_{m=1}^{\infty} \omega_{nmj}\left(X_{jm} r_3^{\lambda_m} + Y_{jm} r_3^{-\lambda_m}\right) \\ +\sum\limits_{j=1}^{N_S} 2\cos(n\gamma_j)\sin(n\theta_S/2)\left(\varphi_{j+1}^F - \varphi_j^F\right)/(n^2\theta_S) \end{array} \right] /\pi,$$

$$T = \theta_S + \theta_F, \gamma_j = (\alpha_j + \beta_{j+1})/2,$$

$$\tau_{nmj} = \begin{cases} \frac{\lambda_m(\cos m\pi \cos n\beta_{j+1} - \cos n\alpha_j)}{n^2 - \lambda_m^2} & \text{if } n \ne \lambda_m \\ \frac{\cos n\alpha_j - \cos m\pi \cos n\beta_j}{2(n+\lambda_m)} - \frac{\theta_S \sin \lambda_m \alpha_j}{2} & \text{if } n = \lambda_m \end{cases}, \text{ and}$$

$$\omega_{nmj} = \begin{cases} \frac{\lambda_m(\cos m\pi \sin n\beta_{j+1} - \sin n\alpha_j)}{n^2-\lambda_m^2} & \text{if } n \neq \lambda_m \\ \frac{\sin n\alpha_j - \cos m\pi \sin n\beta_j}{2(n+\lambda_m)} + \frac{\theta_S \cos \lambda_m \alpha_j}{2} & \text{if } n = \lambda_m \end{cases}.$$

Thus, from (19) and (51), it yields:

$$E_0 \ln r_3 + F_0 = c_0/2 \tag{52}$$

$$E_n r_3^n + F_n r_3^{-n} = c_n \tag{53}$$

$$G_n r_3^n + H_n r_3^{-n} = d_n \tag{54}$$

Moreover, (11) denotes that the continuity of the flux density through this surface should be satisfied. So, after conducting integration with a factor of $\sin \lambda_m(\theta - \alpha_j)$ for both sides of (11), it yields:

$$\int_{\alpha_j}^{\beta_{j+1}} \frac{\partial \varphi_j^S}{\partial r}\Big|_{r=r_3} \sin \lambda_m(\theta-\alpha_j)\mathrm{d}\theta = \int_{\alpha_j}^{\beta_{j+1}} \frac{\partial \varphi^{II}}{\partial r}\Big|_{r=r_3} \sin \lambda_m(\theta-\alpha_j)\mathrm{d}\theta \tag{55}$$

Substituting (19) and (37) into (55), it yields:

$$\frac{m\pi}{2}\left(X_{jm} r_3^{\lambda_m} - Y_{jm} r_3^{-\lambda_m}\right) = \sum_{n=1}^{\infty} n\left[\left(E_n r_3^n - F_n r_3^{-n}\right)\tau_{nmj} + \left(G_n r_3^n - H_n r_3^{-n}\right)\omega_{nmj}\right] + \frac{(1-\cos m\pi)E_0}{\lambda_m} \tag{56}$$

Fifthly, on the outside surface of the stationary ring, the following equations can be similarly deduced:

$$I_0 \ln r_4 + J_0 = e_0/2 \tag{57}$$

$$I_n r_4^n + J_n r_4^{-n} = e_n \tag{58}$$

$$K_n r_4^n + L_n r_4^{-n} = f_n \tag{59}$$

$$\frac{m\pi}{2}\left(X_{jm} r_4^{\lambda_m} - Y_{jm} r_4^{-\lambda_m}\right) = \sum_{n=1}^{\infty} n\left[\left(I_n r_4^n - J_n r_4^{-n}\right)\tau_{nmj} + \left(K_n r_4^n - L_n r_4^{-n}\right)\omega_{nmj}\right] + \frac{(1-\cos m\pi)I_0}{\lambda_m} \tag{60}$$

where

$$e_0 = \left[\begin{array}{l} \sum_{j=1}^{N_S}\sum_{m=1}^{\infty}(1-\cos m\pi)\left(X_{jm} r_4^{\lambda_m} + Y_{jm} r_4^{-\lambda_m}\right)/\lambda_m \\ +T\sum_{j=1}^{N_S}\varphi_j^F \end{array}\right]/\pi,$$

$$e_n = \left[\begin{array}{l} \sum\limits_{j=1}^{N_S} \sum\limits_{m=1}^{\infty} \tau_{nmj} \left(X_{jm} r_4^{\lambda_m} + Y_{jm} r_4^{-\lambda_m} \right) \\ - \sum\limits_{j=1}^{N_S} 2\sin(n\gamma_j) \sin(n\theta_S/2) \left(\varphi_{j+1}^F - \varphi_j^F \right) / (n^2\theta_S) \end{array} \right] /\pi, \text{ and}$$

$$f_n = \left[\begin{array}{l} \sum\limits_{j=1}^{N_S} \sum\limits_{m=1}^{\infty} \omega_{nmj} \left(X_{jm} r_4^{\lambda_m} + Y_{jm} r_4^{-\lambda_m} \right) \\ + \sum\limits_{j=1}^{N_S} 2\cos(n\gamma_j) \sin(n\theta_S/2) \left(\varphi_{j+1}^F - \varphi_j^F \right) / (n^2\theta_S) \end{array} \right] /\pi.$$

Finally, the continuity of flux across the ferromagnetic segments should also be taken into consideration. Fig. 5 illustrates the flux across the stationary ring and each ferromagnetic segment. In Fig. 5(a), the flux flowing through the inside surface and the outside surface should be equal:

$$\oint \frac{\partial \varphi^{II}}{\partial r}\Big|_{r=r_3} r\mathrm{d}\theta = \oint \frac{\partial \varphi^{III}}{\partial r}\Big|_{r=r_4} r\mathrm{d}\theta \tag{61}$$

Substituting (19) and (20) into (61), it yields:

$$E_0 = I_0 \tag{62}$$

In Fig. 5(b), the flux flowing into the ferromagnetic segment should be equal to that flowing out of it. So, it yields:

$$\begin{array}{l} \int_{\beta_j}^{\alpha_j} -\frac{\partial \varphi^{II}}{\partial r}\Big|_{r=r_3} \mathrm{d}\theta + \int_{r_3}^{r_4} -\frac{\partial \varphi_{j-1}^S}{r\partial\theta}\Big|_{\theta=\beta_j} \mathrm{d}\theta \\ = \int_{\beta_j}^{\alpha_j} -\frac{\partial \varphi^{III}}{\partial r}\Big|_{r=r_4} \mathrm{d}\theta + \int_{r_3}^{r_4} -\frac{\partial \varphi_j^S}{r\partial\theta}\Big|_{\theta=\alpha_j} \mathrm{d}\theta \end{array} \tag{63}$$

Substituting (19), (20) and (37) into (63), it yields:

$$\begin{array}{l} \sum\limits_{n=1}^{\infty} 2\sin\left(\frac{n\theta_F}{2}\right) \left[\begin{array}{l} \left(E_n r_3^n - F_n r_3^{-n} - I_n r_4^n + J_n r_4^{-n}\right)\cos(n\eta_j) \\ + \left(G_n r_3^n - H_n r_3^{-n} - K_n r_4^n + L_n r_4^{-n}\right)\sin(n\eta_j) \end{array} \right] = \\ \sum\limits_{m=1}^{\infty} \left[\begin{array}{l} \left(X_{jm} - X_{(j-1)m}\cos m\pi\right)\left(r_4^{\lambda_m} - r_3^{\lambda_m}\right) + \\ \left(Y_{jm} - Y_{(j-1)m}\cos m\pi\right)\left(r_4^{-\lambda_m} - r_3^{-\lambda_m}\right) \end{array} \right] + (\alpha_j - \alpha_{j-1}) \ln\left(\frac{r_4}{r_3}\right) \end{array} \tag{64}$$

where $\eta_j = (\alpha_j + \beta_j)/2$.

Therefore, the unknown quantities A_n, B_n, C_n, D_n, E_n, F_n, G_n, H_n, I_n, J_n, K_n, L_n, A_0, B_0, E_0, F_0, I_0, J_0, X_{jm}, Y_{jm} and φ_j^S that are involved in the scalar magnetic potential solutions can be determined by (38)–(49), (52)–(54), (56)–(60), (62) and (64). It should be noted

that, although (64) can deduce five subequations ($j = 1-5$), only four of them are independent of the others.

After solving the magnetic field distribution built up by the inner rotor PMs, the same process can be conducted to obtain the solution of that excited by the outer rotor PMs. Hence, according to the superposition law, the magnetic field distribution built up by both rotors can be obtained. Then, the flux density distributions can be deduced from the scalar potential by using:

$$B_r = -\mu_0 \frac{\partial \varphi}{\partial r} \tag{65}$$

$$B_r = -\frac{\mu_0}{r} \frac{\partial \varphi}{\partial \theta} \tag{66}$$

4. CALCULATION RESULTS

Figure 6 gives the scalar magnetic potential distributions along the inside and outside surfaces of the stationary ring excited by individual rotors. The initial phase angle θ_0 equals zero.

Figure 7 shows the flux density waveforms at the middle of both airgaps produced by the inner rotor PMs. In order to assess the validity of the analytical method, the corresponding results obtained from the FEM are provided for comparison. For the FEM results, they include the FEM (unsat) case that the saturation effect of iron yokes and ferromagnetic segments is neglected, and the FEM (sat) case that the corresponding saturation effect is depicted by the B-H characteristic of the laminated silicon steel (Type 50H470). It can be seen that

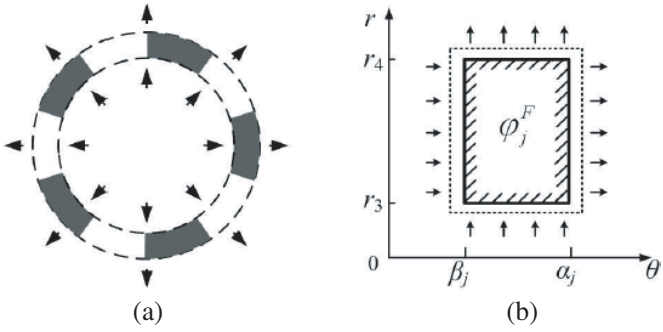

Figure 5. Flux continuity across stationary ring: (a) Whole ring, (b) single ferromagnetic segment.

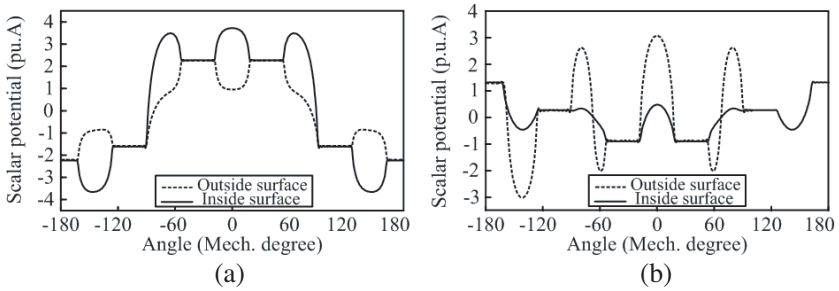

Figure 6. Scalar magnetic potential distributions in stationary ring excited by individual rotors: (a) Inner rotor, (b) outer rotor.

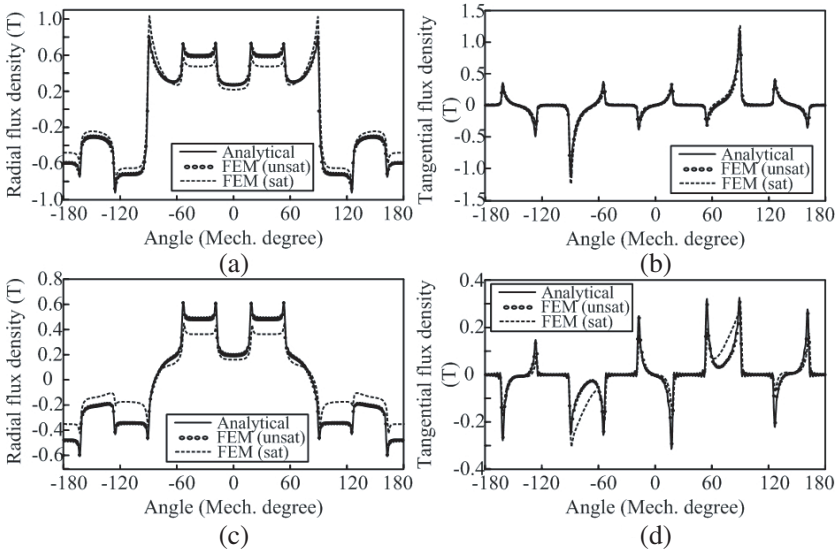

Figure 7. Flux density distributions in both airgaps excited by inner rotor PMs: (a) Radial component in inner airgap, (b) tangential component in inner airgap, (c) radial component in outer airgap, (d) tangential component in outer airgap.

the analytical results agree well with the FEM (unsat) results. On the other hand, the saturation of the ferromagnetic segments has a significant effect on the radial flux density, whereas the effect is less significant on the tangential flux density.

Similarly, the results excited only by the outer rotor PMs are shown in Fig. 8. It can be seen that the analytical results agree well with the FEM (unsat) results. Different from the results excited only by the inner rotor PMs, the saturation of the ferromagnetic segments

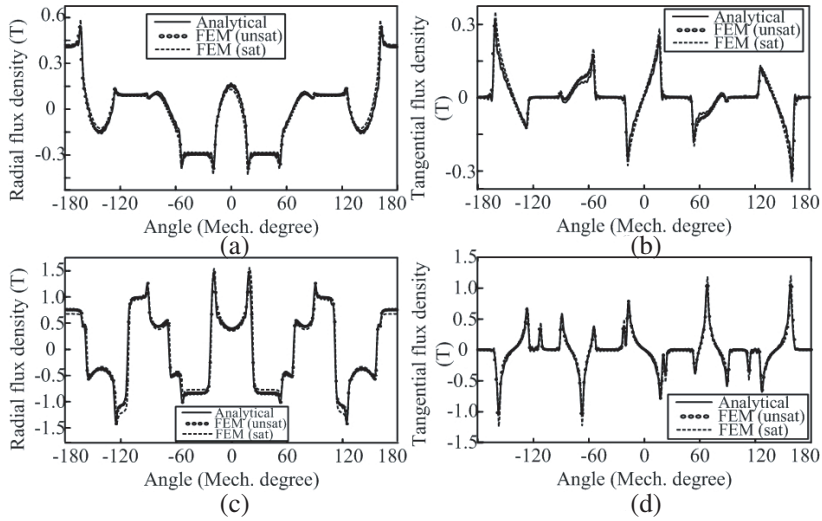

Figure 8. Flux density distributions in both airgaps excited by outer rotor PMs: (a) Radial component in inner airgap, (b) tangential component in inner airgap, (c) radial component in outer airgap, (d) tangential component in outer airgap.

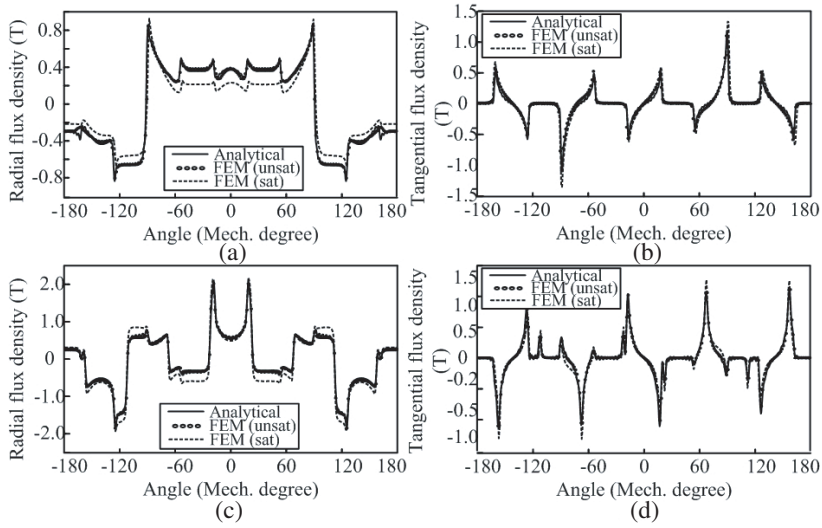

Figure 9. Flux density distributions in both airgaps excited by both rotors: (a) Radial component in inner airgap, (b) tangential component in inner airgap, (c) radial component in outer airgap, (d) tangential component in outer airgap.

has a little effect on both the radial flux density and the tangential flux density. It is due to the fact that the outer rotor has more PM poles than the inner rotor, and the magnetic path is shorter. By summing up these two groups of results, the magnetic field distribution in both airgaps caused by the two rotor PMs together are shown in Fig. 9.

In order to assess the difference of computational resources between the proposed analytical calculation algorithm and the FEM algorithm, they are run by a standard PC (Pentium 4, 3.4 GHz, 1 GB RAM) to generate the required flux density distributions. The corresponding computational time for the proposed algorithm takes only 1.9 s, whereas that for the FEM algorithm is 21 s which is 11 times longer than the proposed one. It should be noted that the required computational time for the FEM calculation has already ignored the time for pre-processing such as mesh generation; otherwise, the required time is much longer.

5. CONCLUSIONS

In this paper, an analytical approach to calculate the magnetic field distribution in coaxial magnetic gears has been proposed and verified. Firstly, a set of partial differential equations in terms of scalar magnetic potential is used to describe the field behavior. Then, the scalar magnetic potentials in different regions are determined by considering the boundary constraints. Consequently, the airgap flux densities are derived from the scalar magnetic potentials. All the analytical results agree well with that obtained from the FEM, which makes the proposed analytical approach be a useful tool for design and optimization of the coaxial magnetic gears.

ACKNOWLEDGMENT

This work was supported by a grant (Project No. HKU7105/ 07E) from the Research Grants Council, Hong Kong Special Administrative Region, China.

REFERENCES

1. Atallah, K., S. Calverley, and D. Howe, "Design, analysis and realization of a high-performance magnetic gear," *IEE Proc. Electric Power Appl.*, Vol. 151, No. 2, 135–143, 2004.
2. Chau, K. T., D. Zhang, J. Z. Jiang, and L. Jian, "Transient analysis of coaxial magnetic gears using finite element comodeling," *Journal of Applied Physics*, Vol. 103, No. 7, 1–3, 2008.

3. Liu, X., K. T. Chau, J. Z. Jiang, and C. Yu, "Design and analysis of interior-magnet outer-rotor concentric magnetic gears," *Journal of Applied Physics*, Vol. 105, No. 7, 1–3, 2009.
4. Furlani, E. P., "A two-dimensional analysis for the coupling of magnetic gears," *IEEE Trans. Mag.*, Vol. 33, No. 3, 2317–2321, 1997.
5. Chau, K. T., D. Zhang, J. Z. Jiang, C. Liu, and Y. Zhang, "Design of a magnetic-geared outer-rotor permanent-magnet brushless motor for electric vehicles," *IEEE Trans. Mag.*, Vol. 43, No. 6, 2504–2506, 2007.
6. Jian, L, K. T. Chau, and J. Z. Jiang, "A magnetic-geared outer-rotor permanent-magnet brushless machine for wind power generation," *IEEE Trans. Ind. Appli.*, in Press.
7. Faiz, J and B. M. Ebrahimi, "Mixed fault diagnosis in three-phase squirrel-cage induction motor using analysis of air-gap magnetic field," *Progress In Electromagnetics Research*, PIER 64, 239–255, 2006.
8. Faiz, J, B. M. Ebrahimi, and M. B. B. Sharifian, "Time stepping finite element analysis of broken bars fault in a three-phase squirrel-cage induction motor," *Progress In Electromagnetics Research*, PIER 68, 53–70, 2007.
9. Ravaud, R., G. Lemarquand, V. Lemarquand, and C. Depollier, "The three exact components of the magnetic field created by a radially magnetized tile permanent magnet," *Progress In Electromagnetics Research*, PIER 88, 307–319, 2008.
10. Babic, S. I. and C. Akyel, "Improvement in the analytical calculation of the magentic field produced by permanent magnet rings," *Progress In Electromagnetics Research*, PIER 5, 71–82, 2008.
11. Ravaud, R., G. Lemarquand, V. Lemarquand, and C. Depollier, "Discussion about the analytical calculation of the magnetic field create by permanent magnets," *Progress In Electromagnetics Research*, PIER 11, 281–297, 2009.
12. Ravaud, R. and G. Lemarquand, "Modelling an ironless loudspeaker by using three-dimensional analytical approach," *Progress In Electromagnetics Research*, PIER 91, 53–68, 2009.
13. Liu, Z. J. and J. T. Li, "Analytical solution of air-gap field in permanent-magnet motors taking into account the effect of pole transition over slots," *IEEE Trans. Magn.*, Vol. 43, No. 10, 3872–3883, 2007.